The Six Isomers of the Cyclohexanol Dimer: A Delicate Test for Dispersion Models

*Marcos Juanes, Imanol Usabiaga, Iker León, Luca Evangelisti, José A. Fernández, Alberto Lesarri**

[*] Mr. M. Juanes, Dr. I. León, Prof. Dr. Alberto Lesarri.
Departamento de Química Física y Química Inorgánica, Universidad de Valladolid, Paseo de Belén, 7, 47011 Valladolid (Spain)

Dr. I. Usabiaga, Dr. I. León, Prof. Dr. J. A. Fernández,
Departamento de Química Física, Universidad del País Vasco, Ap. 644, 48080 Bilbao (Spain)

Dr. L. Evangelisti, Dipartimento di Chimica "G. Ciamician", Università di Bologna, Via Selmi, 2, 40126 Bologna (Italy)

Supporting information can be found under: https://x

Abstract: *The cyclohexanol homodimer is a delicate test model of the role of dispersive forces in intermolecular association. While phenol produces a single dimer, suppression of π interactions in cyclohexanol results in multiple isomerism, as six competing dimers of the free molecule are observed in a supersonic jet expansion. Rotational spectroscopy reveals accurate structural data, specifically the formation of homo- and heterochiral diasteroisomers and the presence of both equatorial and axial forms in the dimers. Three dispersion-corrected density-functional molecular orbital calculations were tested against the experiment, with B3LYP-D3(BJ) offering good structural reproducibility. However, the prediction of the dimer energetics is largely model-dependent, offering a testbed for validation of computational models.*

Entry for the Table of Contents

The competence between a leading hydrogen bond (HB) and weak dispersive forces produces multiple isomerism in the cyclohexanol dimer, as six different species were observed in a jet expansion.

Chiral recognition is as a pervasive molecular player in biological and supramolecular Chemistry, directly influencing ligand binding and macromolecular assembly.[1] Experiments in gas-phase contribute with structural, dynamical and energetic information on the non-covalent interactions observed in the association of free chiral molecules,[2–4] with the ultimate goal of understanding the molecular basis of enantioselectivity. However, the lack of a general aggregation model, the multiple intermolecular forces, the variety of interaction energies, the cooperative and competitive effects and the need of accurate empirical data to validate quantum mechanical models call for additional experiments on chiral recognition between isolated molecules.

Chiral recognition is primarily affected by the stereomutation barriers. Low stereomutation barriers are denoted transient chirality and the molecular recognition process, which might involve a structural readaptation, has been categorized as chirality synchronization.[2] Homodimers with transient chirality are interesting because the formation of the cluster quenches stereomutation, offering the possibility to detect separately the hetero- and homochiral diastereomeric clusters and insights into the recognition process.

Torsional chirality has been mostly studied in alcohols, because of the moderately strong O-H···O H-bond and the use of the O-H stretching vibration as structural probe in IR,[5] Raman,[6] IR/UV[7,8] or IR/IR/IR[9] spectroscopy. Microwave spectroscopy offers higher (sub-Doppler) resolution, unambiguous structural identification and general applicability.[4,10] However, the number of rotational studies on transiently chiral dimers is scarce.[11–19] The analysis of the cyclohexanol dimer explores the balance of intermolecular forces and the differences with phenol.[20] Our results reveal a rich isomerism, arising unexpected questions. In particular, how non-covalent forces affect

isomerism? Can density functional theory (DFT) account for the energetics and structure? and, finally, can you invert a cyclohexanol ring in a jet expansion?

Cyclohexanol offers a variety of structural families, based on axial (A) /equatorial (E) inversion chairs and large-amplitude vibration of the hydroxyl group in Figure 1. The most stable equatorial conformer is a fluxional structure tunneling between two symmetry-equivalent equatorial-gauche (EG+ and EG-) isomers, splitting the ground-vibrational state into two torsional-rotation sublevels (ΔE_{01}=52(2) GHz).[21] The equatorial-trans (ET) conformer adopts a non-degenerate rigid structure. The axial conformers (ca. 2-6 kJ mol^{-1}), previously observed for 3-methylcyclohexanol,[22] were not detected for cyclohexanol.[21] On formation of the cyclohexanol dimer the gauche stereomutation is broken and the two enantiomers become distinguishable, producing distinct diastereoisomers. Assuming that the dimer is primary stabilized by a conventional O-H···O hydrogen bond, the two oxygen lone-pairs in the proton acceptor offer six (2 E/A and 3 G+/G-/T) possibilities for each of the six proton donor cases, forming 72 isomer families in 36 enantiomeric pairs. However, previous vibrational investigations could only identify a single EG-EG isomer.[9] Recent FTIR and Raman jet spectra have suggested at least four isomers,[23] demanding conclusive investigations.

Cyclohexanol was first probed in a neon jet expansion using broadband chirped-pulsed microwave spectroscopy[24,25] (see Supporting Information, SI). The spectrum in Figures 2 and S1-S2 (SI) is dominated by the monomer, but contains other weak (5-10%) features from plausible clusters. The spectral assignment started from trial rotational constants and iteratively led to the identification of six isomers of the homodimer (I-VI). The rotational transitions (Tables S1-S6, SI) were fitted to a semirigid-rotor Hamiltonian, with spectroscopic parameters in Table 1. A second experiment in helium did not identify additional species. Experiments with argon showed only isomers II, III and IV,

confirming that the global minimum is one of these species and the presence of conformational relaxation.[10]

The experiment was rationalized with molecular orbital calculations. The PES was expected quite shallow and corrugated, with multiple local minima of small energy, low isomerization barriers and multiple interconversion paths. Our computational strategy (SI) used DFT to probe the maximum conformational space.[26,27] Following molecular mechanics screening (203 isomers), the 60 most stable structures were reoptimized with three hybrid or meta-GGA functionals, including B3LYP,[28] MN15-L[29] and M06-2X,[30] using Ahlrichs' polarized triple-zeta basis def2-TZVP. [31] Minnesota functionals were assumed parametrized for dispersion. B3LYP was supplemented with D3[32] dispersion corrections and Becke-Johnson damping.[33] Finally, the isomers located with each method were reoptimized with the other two functionals. Convergence difficulties were apparent, with minor changes in the initial geometries resulting in different final structures. Tables S7-S9 (SI) collect the computational results.

All observed isomers could be identified with one of the predicted structures. However, the three DFT methods approximate the experiment differently. MN15-L and M06-2X behaved similarly and reproduced the rotational constants with larger relative deviations (~2.0-5.0%). B3LYP-D3(BJ) offered the best agreement, with maximum relative deviations below 3% (i.e., IV and V) and best agreements of 0.1-1.0% (i.e., III and VI). Table S10 (SI) compares experiment and theory for B3LYP-D3(BJ). The results support the argument that Minnesota functionals might need corrections for long-range dispersion.[26] Despite the good agreement, both the convergence difficulties and the fact that small structural changes (exchange of donor/acceptor or hydroxyl internal rotation) may produce similar rotational constants and conformational energies, turn the structural

conclusions model-dependent. Convergence difficulties were confirmed a posteriori by an independent search using PW6B95-D3.[34,35]

Isomer identification is given in Table 1 and Figure 3, with labels indicating the equatorial/axial and gauche/trans orientations for the proton donor and acceptor, respectively, the (+/-) gauche chirality (relative to a $^1C_4$ chair) and the bridging oxygen lone pair position (1/2) at the proton acceptor. The equatorial-gauche appears in all isomers, as expected from its larger stability in the monomer. However, one of the two monomers occasionally adopts other geometries (see 3-D Figures S3-S8 and Tables S11-S16, SI). Specifically, three isomers contain an axial-gauche moiety (III=EG-(1)AG-, IV=EG-(1)AG+, V=AG-(1)EG+) and one isomer contains the axial-trans orientation (I=AT(2)EG-). The two remaining isomers are composed exclusively of equatorial-gauche forms (II=EG-(2)EG-, VI=EG-(1)EG+). The present computational model and the spectral intensities give population ratios of I:II:III:IV:V:VI = 1.0(4):0.7(4):0.6(3): 0.5(2):0.3(1):0.3(1). This calculation is only approximate, as it additionally assumes a polarization regime proportional to the squared dipole moments and uniform instrumental response.[25]

The presence of axial forms is noticeable. Unlike 1-methylcyclohexanol, where the bulkier methyl group stabilizes the axial hydroxyl,[22] cyclohexanol has preference for the equatorial conformations (Figure S9, SI). [21] In order to explain the axial forms we compared the equatorial-to-axial potential barriers both in the monomer and the dimer. The inversion barrier for the cyclohexanol chair was predicted as 47-54 kJ mol^{-1} in Figure S10 (SI). A similar calculation in the dimer starting from each of the observed geometries and averaging over six inversion paths rendered comparatively similar barriers of 44-51 kJ mol^{-1} in Figure S11 (SI). We conclude that there are no plausible ring inversion paths of reduced energy, so the presence of axial forms is due to energetic collisions at the

initial stages of the expansion. Collisional stabilization of specific isomers undetected in the monomers has been observed in jets for other clusters. [36–38]

The intermolecular interactions have been mapped using non-covalent-interactions plots in Figures 4 and S12-S17 (SI), based on a reduced gradient $s\left(=\frac{1}{1(3\pi^2)^{1/3}}\frac{|\nabla\rho|}{\rho^{4/3}}\right)$ of the electron density.[39] All the observed structures exhibit an O-H···O hydrogen bond with predicted distances r_e=1.891-1.904 Å (B3LYP-D3(BJ)), except for the AT proton donor (1.948 Å). In some isomers additional weak C-H···O hydrogen bonds are apparent (2.65-2.82 Å). In all cases, the two cyclohexyl moieties avoid near-stacking structures. The hydrogen bond distance is intermediate between the phenol dimer[20] (O···H: r_0=1.837(23)-1.879(38) Å, r_e=1.87-89 Å; O···O: r_0=2.830(36)-2.833(21) Å) and the water dimer (O···O: r_0=2.976 Å, r_e=2.952 Å). Additional insight into the nature of the non-covalent interactions was obtained by energy decomposition. SAPT(0) results in Table S17 (SI) show that while the primary interaction in both cases is electrostatic and accounts for a similar contribution (144%) to the binding energy, the dispersion component is much larger in cyclohexanol than in phenol (122% vs 73%).

In conclusion, we characterized the association between two neutral free molecules of cyclohexanol in a jet expansion. Compared to the phenol dimer, [20] the suppression of π-π or C-H···π stabilization forces results in weaker interactions and multiple isomerism. The alcohol stereomutation is quenched in the dimers, so the gauche chiral species collapse into different diastereoisomers. However, there is no indication of a dominant stereoselectivity as both homochiral and heterochiral species are observed in the dimer. In other small-alcohol dimers both homochiral[11,12] and heterochiral[13,14,17] preferences have been observed, anticipating sensitive isomerization equilibria in shallow multiconformational PES.

Because of the competition between multiple low-energy species the computational survey was of difficult convergence. Moreover, the DFT dimer energetics turned out model-dependent and show deficiencies to assess the observed minima. In this sense, the cyclohexanol dimer proves an interesting testbed for the predictability of computational models describing non-covalent interactions. This issue can be related to the most general search of benchmark clusters and appropriate dispersion models within the "DFT zoo", as advocated by Grimme.[26] This result evidences how the combination of rotational data with computational methods offers a synergic benefit to characterize weakly-bound chirality recognition models in gas phase.

Acknowledgements

Funding from the Spanish MICINN-FEDER (PGC2018-098561-B-C22) s gratefully acknowledged.

Keywords: Homodimers, Molecular recognition, Hydrogen bonding, Rotational spectroscopy, Jet spectroscopy.

REFERENCES

[1] S. M. Morrow, A. J. Bissette, S. P. Fletcher, *Nat. Nanotechnol.* **2017**, *12*, 410–419.

[2] A. Zehnacker, M. A. Suhm, *Angew. Chemie - Int. Ed.* **2008**, *47*, 6970–6992.

[3] A. Zehnacker, Ed. , *Chiral Recognition in the Gas Phase*, CRC Press, Boca Raton, Florida, **2010**.

[4] M. Juanes, R. T. Saragi, W. Caminati, A. Lesarri, *Chem. - A Eur. J.* **2019**, *25*, 11402–11411.

[5] T. B. Adler, N. Borho, M. Reiher, M. A. Suhm, *Angew. Chemie - Int. Ed.* **2006**, *45*, 3440–3445.

[6] T. N. Wassermann, P. Zielke, J. J. Lee, C. Cézard, M. A. Suhm, *J. Phys. Chem. A* **2007**, *111*, 7437–7448.

[7] I. Usabiaga, A. Camiruaga, C. Calabrese, A. Maris, J. A. Fernández, *Chem. - A Eur. J.* **2019**, *25*, 14230–14236.

[8] A. M. Rijs, J. Oomens, in *Gas-Phase IR Spectrosc. Struct. Biol. Mol.* (Eds.: A.M. Rijs, J. Oomens), Springer International Publishing, Cham, **2015**, pp. 1–42.

[9] I. León, R. Montero, A. Longarte, J. A. Fernández, *J. Chem. Phys.* **2013**, *139*, 174312.

[10] W. Caminati, J.-U. Grabow, in *Front. Adv. Mol. Spectrosc.* (Ed.: J. Laane), Elsevier Inc., **2018**, pp. 569–598.

[11] J. P. I. Hearn, R. V. Cobley, B. J. Howard, *J. Chem. Phys.* **2005**, *123*, 1–7.

[12] D. Loru, I. Peña, M. E. Sanz, *J. Mol. Spectrosc.* **2017**, *335*, 93–101.

[13] M. S. Snow, B. J. Howard, L. Evangelisti, W. Caminati, *J. Phys. Chem. A* **2011**, *115*, 47–51.

[14] A. K. King, B. J. Howard, *Chem. Phys. Lett.* **2001**, *348*, 343–349.

[15] Z. Su, N. Borho, Y. Xu, *J. Am. Chem. Soc.* **2006**, *128*, 17126–17131.

[16] A. Maris, B. M. Giuliano, D. Bonazzi, W. Caminati, *J. Am. Chem. Soc.* **2008**, *130*, 13860–13861.

[17] X. Liu, N. Borho, Y. Xu, *Chem. - A Eur. J.* **2009**, *15*, 270–277.

[18] J. Thomas, Y. Xu, *J. Phys. Chem. Lett.* **2014**, *5*, 1850–1855.

[19] N. A. Seifert, C. Pérez, J. L. Neill, B. H. Pate, M. Vallejo-López, A. Lesarri, E. J. Cocinero, F. Castaño, *Phys. Chem. Chem. Phys.* **2015**, *17*, 18282–18287.

[20] N. A. Seifert, A. L. Steber, J. L. Neill, C. Pérez, D. P. Zaleski, B. H. Pate, A. Lesarri, *Phys. Chem. Chem. Phys.* **2013**, *15*, 11468–11477.

[21] M. Juanes, W. Li, L. Spada, L. Evangelisti, A. Lesarri, W. Caminati, *Phys. Chem. Chem. Phys.* **2019**, *21*, 3676–3682.

[22] W. Li, L. Spada, L. Evangelisti, W. Caminati, *J. Phys. Chem. A* **2016**, *120*, 4338–4342.

[23] B. Hartwig, M. Heger, M. A. Suhm, *Private Communication*, **2020**.

[24] S. T. Shipman, B. H. Pate, in *Handb. High-Resolution Spectrosc.* (Eds.: F. Merkt, M. Quack), John Wiley & Sons, Ltd, New York, **2011**, pp. 801–828.

[25] J.-U. Grabow, in *Handb. High-Resolution Spectrosc.* (Eds.: F. Merkt, M. Quack), John Wiley & Sons, Ltd, New York, **2011**, pp. 723–799.

[26] L. Goerigk, A. Hansen, C. Bauer, S. Ehrlich, A. Najibi, S. Grimme, *Phys. Chem. Chem. Phys.* **2017**, *19*, 32184–32215.

[27] M. Juanes, A. Lesarri, R. Pinacho, E. Charro, J. E. Rubio, L. Enríquez, M. Jaraíz, *Chem. - A Eur. J.* **2018**, *24*, 6564–6571.

[28] A. D. Becke, *J. Chem. Phys.* **1993**, *98*, 5648–5652.

[29] H. S. Yu, X. He, D. G. Truhlar, *J. Chem. Theory Comput.* **2016**, *12*, 1280–1293.

[30] Y. Zhao, D. G. Truhlar, *Theor. Chem. Acc.* **2008**, *120*, 215–241.
[31] F. Weigend, R. Ahlrichs, *Phys. Chem. Chem. Phys.* **2005**, *7*, 3297–3305.
[32] S. Grimme, J. Antony, S. Ehrlich, H. Krieg, *J. Chem. Phys.* **2010**, *132*, 1–19.
[33] S. Grimme, S. Ehrlich, L. Goerigk, *J. Comput. Chem.* **2011**, *32*, 1456–1465.
[34] S. Grimme, *Private Communication*, **2020**.
[35] C. Bannwarth, S. Ehlert, S. Grimme, *J. Chem. Theory Comput.* **2019**, *15*, 1652–1671.
[36] J. Thomas, N. A. Seifert, W. Jäger, Y. Xu, *Angew. Chemie - Int. Ed.* **2017**, *56*, 6289–6293.
[37] N. A. Seifert, J. Thomas, W. Jäger, Y. Xu, *Phys. Chem. Chem. Phys.* **2018**, *20*, 27630–27637.
[38] S. Oswald, N. A. Seifert, F. Bohle, M. Gawrilow, S. Grimme, W. Jäger, Y. Xu, M. A. Suhm, *Angew. Chemie - Int. Ed.* **2019**, *58*, 5080–5084.
[39] E. R. Johnson, S. Keinan, P. Mori-Sánchez, J. Contreras-García, A. J. Cohen, W. Yang, *J. Am. Chem. Soc.* **2010**, *132*, 6498–6506.

Figure 1. Large-amplitude motions in the cyclohexanol monomer.

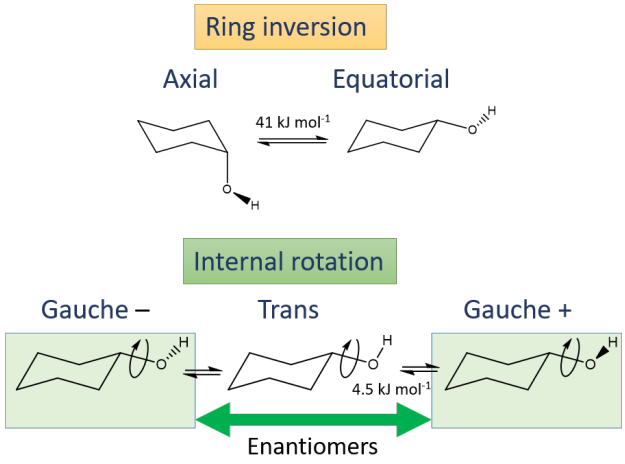

Figure 2. The microwave spectrum of the cyclohexanol dimer and a 120 MHz expansion, showing transitions from six different isomers.

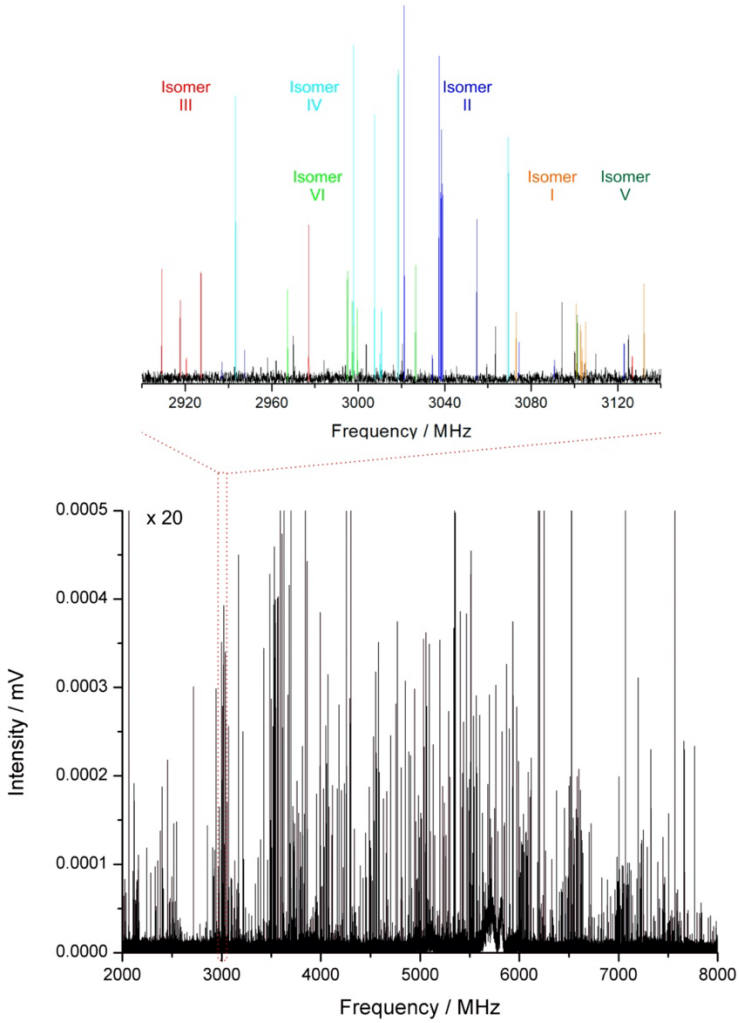

Figure 3. Conformational assignment of the six isomers of the cyclohexanol dimer and hydrogen bond distances according to B3LYP-D3(BJ).

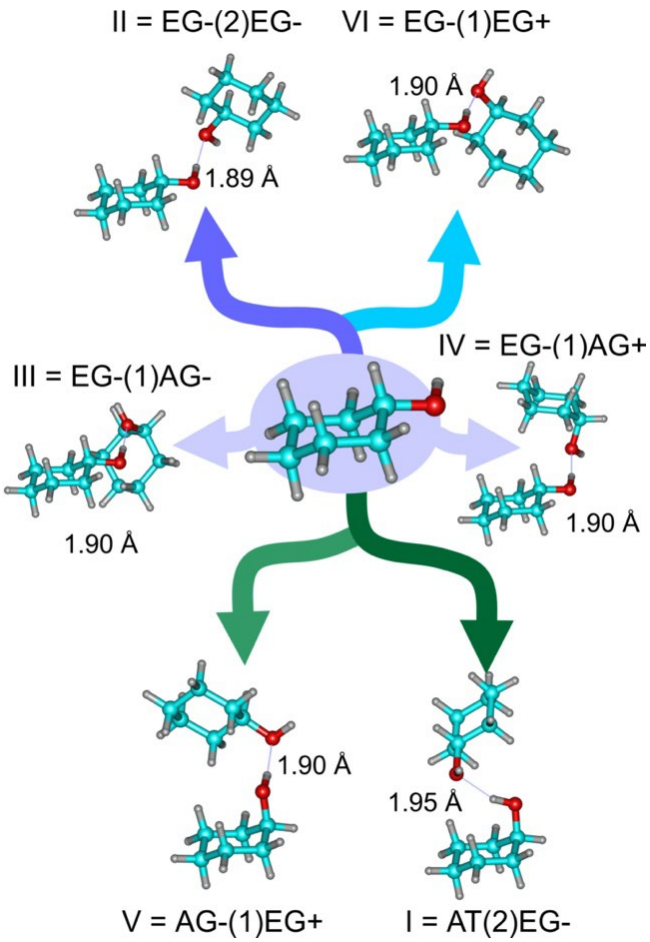

Figure 4. The spatial distribution of the non-covalent interactions in isomer IV of the cylohexanol dimer, according to a NCIPlot analysis. The O-H···O H-bond (blue) is accompanied by broad weak dispersive interactions (green shades) and repulsive zones (red). The lower graphic shows the reduced electronic density gradient representation for the water (blue), phenol (green) and cyclohexanol dimers (red), see SI.

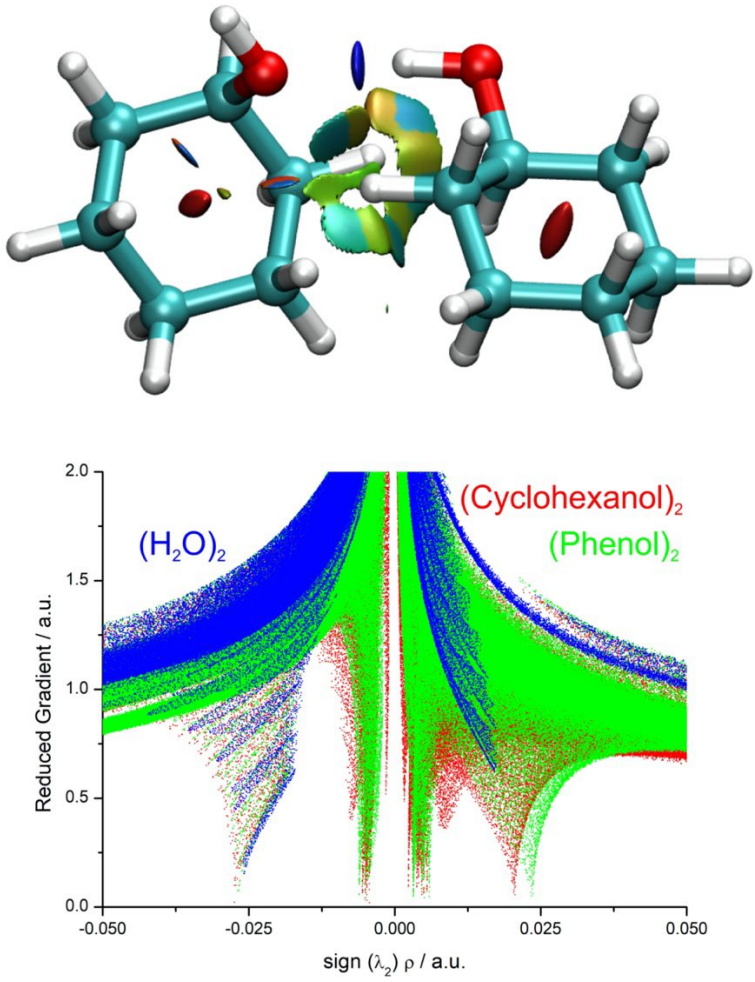

Table 1. Rotational parameters for isomers I-VI of the cyclohexanol dimer.

	Isomer I	Isomer II	Isomer III	Isomer IV	Isomer V	Isomer VI
	AT(2)EG-	EG-(2)EG-	EG-(1)AG-	EG-(1)AG+	AG-(1)EG+	EG-(1)EG+
A / MHz[a]	1218.11(23)[c]	1273.9599(22)	1203.5721(82)	1167.877(41)	1039.694(67)	1311.72(22)
B / MHz	316.22133(97)	255.99343(18)	303.99025(48)	313.51209(51)	328.52277(90)	254.73673(31)
C / MHz	304.41165(91)	250.38848(19)	279.76964(43)	288.25106(51)	304.34728(85)	244.86010(34)
D_J / kHz	0.0583(13)	0.05908(57)	0.06469(69)	0.06942(56)	0.2037(13)	0.06438(54)
D_{JK} / kHz	-0.1976(88)	-0.4638(99)	-0.2661(34)	-0.2290(26)	-0.475(11)	-0.5107(72)
D_K / kHz	[0.0]	1.45(34)	[0.0]	[0.0]	[0.0]	[0.0]
d_1 / kHz	-0.0043(19)	[0.0]	-0.01083(87)	-0.01058(97)	-0.0286(20)	[0.0]
N[b]	71	129	101	106	69	100
σ / kHz	13.0	13.3	10.3	8.3	12.2	13.5

[a]Rotational constants (A, B, C) and Watson's S-reduction centrifugal distortion constants (D_J, D_{JK}, D_K, d_1, d_2=[0.0])
[b]Number of transitions (N) and rms deviation (σ) of the fit. [c]Standard errors in units of the last digit.